JOURNAL OF PROPULSION AND POWER
Vol. 20, No. 5, September–October 2004

Unsteady Effects on Ram Accelerator Operation at Elevated Fill Pressures

C. Bundy,* C. Knowlen,† and A. P. Bruckner‡
University of Washington, Seattle, Washington 98195-2250

Experiments show that as the projectile acceleration of the ram accelerator is increased, by increasing the propellant fill pressure or reducing the projectile mass, its performance begins to deviate significantly from that predicted by the widely used quasi-steady control volume model. At high fill pressures, experimental velocity–distance data are overpredicted by the quasi-steady model for thrust determination when using a real-gas equation of state for the combustion products. The primary reason for this behavior is that the mass of the propellant accumulating in the control volume at high fill pressure approaches the mass of the projectile itself. A revision to the control volume model to account for unsteady flow effects indicates that the thrust coefficient vs Mach-number profile obtained for high-pressure conditions is consistently lower than that obtained with the quasi-steady model. This deviation correlates with experimental results obtained in a 38-mm-bore ram accelerator at fill pressures in the range of 15–20 MPa. The best agreement with high-pressure experimental data is obtained using the unsteady modeling approach in conjunction with the heat release vs Mach-number profile calculated using the Boltzmann equation of state.

Nomenclature

A	=	area (cross sectional or surface)
a	=	acceleration
c	=	acoustic speed
c_p	=	specific heat capacity at constant pressure
e	=	specific internal energy
F	=	net thrust force
h	=	specific enthalpy
I	=	thrust coefficient, $=F/P_1A$
L	=	length
M	=	Mach number
m	=	mass
$\dot{m}$	=	mass flow rate
P	=	pressure
Q	=	nondimensional heat-release parameter, $=\Delta q/(c_pT_1)$
R	=	gas constant
s	=	specific entropy
T	=	temperature
t	=	time
u	=	velocity
V	=	volume
v	=	specific volume
x	=	distance
γ	=	ratio of specific heat capacities
Δ	=	change in parameter
Δq	=	specific heat release
ρ	=	density
σ	=	compressibility coefficient
τ	=	characteristic time

Subscripts

CJ	=	Chapman–Jouguet condition
CV	=	control volume
g	=	gas
p	=	projectile
0	=	total or stagnation condition
1	=	control volume inlet condition
2	=	control volume exit condition

Introduction

THE ram accelerator is a hypervelocity launcher that uses in-tube ramjet-like propulsive cycles to generate thrust for projectiles.[1] A stationary tube, analogous to the outer cowling of a ramjet engine, is filled with a pressurized, combustible gas mixture that is contained by thin diaphragms. A subcaliber projectile, similar in shape to the centerbody of a supersonic ramjet, is injected, with a lightweight obturator attached to its base, into the ram accelerator by a conventional gun-type launcher. The gasdynamic process that occurs as the projectile and obturator enter the ram accelerator detaches the obturator from the projectile, establishes a supersonic flowfield around the forebody of the projectile, and initiates combustion on or behind it.[2,3] This process generates high projectile base pressure, which results in continuous acceleration at supersonic speed. Thrust increases with fill pressure and propellant heat release; thus, the highest possible acceleration performance for a given projectile mass is obtained by using the maximum fill pressure that the launch facility can accommodate, along with the most energetic propellant that will sustain ram accelerator operation at that pressure.

An experimental and theoretical research program has been carried out to determine operating parameters for which continuous ram accelerator operation is possible at propellant fill pressures up to 20 MPa and to accurately model the performance obtained under such conditions. The effects of projectile acceleration and real-gas behavior need to be taken into account to completely determine the thrust of the one-dimensional model for the thermally choked ram accelerator propulsive mode. This research is an essential precursor to the development of ram accelerator launch systems, which will require fill pressures of 10–50 MPa to generate high thrust for applications such as direct space launch and military defense.[4,5]

Theoretical Modeling

The prediction for axial force (thrust) acting on a ram accelerator projectile is dependent on the propellant composition, fill pressure,

Received 18 December 2002; revision received 23 January 2004; accepted for publication 8 February 2004. Copyright © 2004 by the American Institute of Aeronautics and Astronautics, Inc. All rights reserved. Copies of this paper may be made for personal or internal use, on condition that the copier pay the $10.00 per-copy fee to the Copyright Clearance Center, Inc., 222 Rosewood Drive, Danvers, MA 01923; include the code 0748-4658/04 $10.00 in correspondence with the CCC.

*Graduate Student; currently Technical Services, at Epic Systems Corporation Madison, Wisconsin 53711. Member AIAA.

†Research Scientist, Department of Aeronautics and Astronautics. Associate Fellow AIAA.

‡Professor and Department Chair, Department of Aeronautics and Astronautics. Fellow AIAA.

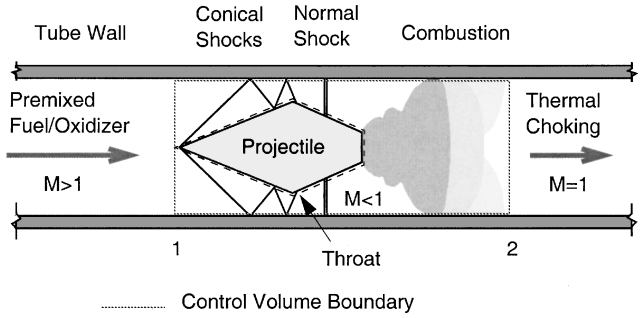

Fig. 1 Thermally choked ram accelerator propulsive mode.

equations of state for reactants and products, the Mach number of the projectile relative to the quiescent propellant, and unsteady effects due to high rates of projectile acceleration. This section presents the quasi-steady and unsteady one-dimensional theoretical models. A sensitivity analysis of the unsteady model with respect to heat release, pressure ratio, and acoustic speed at the thermal choke point is provided in the Appendix.

Quasi-Steady Real Gas Effects

The theoretical thrust of the thermally choked propulsive mode is readily determined in the reference frame of the projectile by applying the steady, one-dimensional gasdynamic conservation equations to the entrance and exit planes of an appropriately chosen control volume, as shown in Fig. 1, and assuming that the exit flow is at sonic speed with respect to the projectile.[6,7] If the projectile geometry and velocity are such that the flow properties at the exit of the control volume correspond to a thermally choked state, then the theoretical thrust is independent of projectile geometry.[8] Real-gas effects are incorporated with a compressibility term σ in the ideal-gas equation of state as follows: $P = \sigma\rho RT$ (Ref. 9). This modeling approach enables an analytical expression to be readily determined for ram accelerator thrust, which incorporates the real-gas correction term.[10]

A computer code that can accommodate several different equations of state to investigate real-gas effects on the temperature, pressure, and chemical equilibria of the products at the thermal choking point has been developed.[11] Fugacity coefficients are used to evaluate shifts in chemical equilibria caused by molecular interactions and finite volumes.[12] For the purposes of this paper, real-gas effects are evaluated with the Boltzmann virial expansion of the equation of state.[9,10] The general effect of modeling with a real-gas equation of state is that the predicted thrust coefficient is increased as a result of increases in the calculated heat release, pressure ratio across the control volume, and acoustic speed at the thermal choking plane. The calculated variation with Mach number of these parameters as a result of incorporating real-gas effects is discussed in Ref. 13.

The one-dimensional theoretical model has several limitations, which must be considered when interpreting the results. First of all, this model does not account for the presence of an obturator and thus cannot provide insight on the experimental conditions needed to initiate ram accelerator operation. Secondly, the model is exact (in a one-dimensional sense) only when the projectile is not accelerating. At high fill pressure, the ratio of propellant density to projectile density becomes nontrivial,[6,14] resulting in a higher fraction of the chemical energy being used to accelerate the propellant itself within the control volume. Consequently, the quasi-steady theoretical model overpredicts the thrust, and thus the projectile acceleration, for thermally choked operation at high pressure.[13,15] The model is still useful, however, as a reference for experimental results and to estimate the effects on acceleration performance anticipated with changes in propellant composition, fill pressure, and Mach number.

Effects of Unsteady Flow

To obtain a more accurate prediction of the thrust at high pressures, it becomes necessary to account for the unsteady flow effects that are disregarded in the quasi-steady control volume model. Thus, to investigate the first-order effects of projectile acceleration on the net thrust of the thermally choked ram accelerator propulsive mode, a one-dimensional unsteady flow model was developed, which accounts for the finite length of the combustion zone and the dependency of the amount of heat release on the in-tube Mach number.[16]

The control volume considered for the unsteady analysis is the same as that shown in Fig. 1; however, the exit plane at station 2 is now considered to be at a pre-determined distance with respect to station 1 (which is attached to the projectile nose tip). A projectile-fixed system of coordinates with the positive flow direction to the right is assumed. In the projectile reference frame, the propellant moves toward the projectile at velocity u_1 while accelerating at the rate a_p. The conservation equations can be expressed as[6]

$$\frac{\partial}{\partial t}\int_{\mathrm{CV}} \rho \,\mathrm{d}V + \rho_2 u_2 A - \rho_1 u_1 A = 0 \tag{1}$$

$$\frac{\partial}{\partial t}\int_{\mathrm{CV}} \rho u \,\mathrm{d}V + A\left(P_2 + \rho_2 u_2^2\right) - A\left(P_1 + \rho_1 u_1^2\right) - \int_{\mathrm{CV}} a_p \rho \,\mathrm{d}V - F = 0 \tag{2}$$

$$\frac{\partial}{\partial t}\int_{\mathrm{CV}} \rho\left(e + \frac{u^2}{2}\right)\mathrm{d}V + A\rho_2 u_2\left(h_2 + \frac{u_2^2}{2}\right) + A\rho_1 u_1\left(h_1 + \frac{u_1^2}{2} + \Delta q\right) - \int_{\mathrm{CV}} u a_p \rho \,\mathrm{d}V = 0 \tag{3}$$

Previous analytical studies demonstrated that at high velocities ($\sim$2000 m/s) and modest accelerations ($<$15,000 g), the unsteady terms in the conservation equations have magnitudes on the order of a few percent of the magnitudes of the steady convective terms and thus can be considered negligible.[6,14,17] In this analysis the unsteady terms are retained based on the assumption that at high fill pressures the greater accelerations will increase the magnitude of their effect.

The unsteady term in the continuity equation (1) is the rate of accumulation of mass in the control volume as a result of its acceleration. This term can be estimated by comparing the change in mass flow rate entering the control volume during the residence time τ of a fluid particle in the control volume to the instantaneous mass flow rate at the entrance[6] i.e.,

$$\Delta\dot{m}/\dot{m} = \Delta u_1/u_1 \tag{4}$$

In this relation, $\Delta u_1 = a_p\tau$ is the change in the velocity of the incoming flow during a time interval τ. An appropriate time interval to use is the particle residence time, which can be approximated as $\tau \approx L_{\mathrm{CV}}/u_1$, where L_{CV} is the length of the control volume.[6,18] It follows that

$$\Delta u_1/u_1 = a_p L_{\mathrm{CV}}/u_1^2 \tag{5}$$

The rate of accumulation of mass in the control volume can then be represented as

$$\frac{\partial}{\partial t}\int_{\mathrm{CV}} \rho \,\mathrm{d}V = \Delta\dot{m} = \frac{a_p \rho_1 A L_{\mathrm{CV}}}{u_1} \tag{6}$$

The continuity equation thus becomes

$$a_p \rho_1 A L_{\mathrm{CV}}/u_1 + A\rho_2 u_2 - A\rho_1 u_1 = 0 \tag{7}$$

In the momentum equation (2), the first integral term is the rate of accumulation of momentum in the control volume. Its retention in this analysis indicates that a fraction of the total available momentum is being expended accelerating gas within the control volume rather than accelerating the projectile. The second integral is a body force resulting from the acceleration of the projectile reference frame with respect to the inertial reference frame.[6,18] The term F is the net

force exerted on the control volume by the projectile and is equal in magnitude to the thrust. The first integral term of the momentum equation can be evaluated as follows:

$$\frac{\partial}{\partial t}\int_{\mathrm{CV}} \rho u \,\mathrm{d}V = \int_{\mathrm{CV}} u\frac{\partial \rho}{\partial t}\,\mathrm{d}V + \int_{\mathrm{CV}} \rho\frac{\partial u}{\partial t}\,\mathrm{d}V \tag{8}$$

From the discussion of the continuity equation, it can be shown that[13]

$$\int_{\mathrm{CV}} u\frac{\partial \rho}{\partial t}\,\mathrm{d}V \approx u_1 \Delta\dot{m} = a_p \rho_1 A L_{\mathrm{CV}} \tag{9}$$

The second term of the first integral term can be approximated as

$$\int_{\mathrm{CV}} \rho\frac{\partial u}{\partial t}\,\mathrm{d}V \approx \frac{\partial u_1}{\partial t}\rho_1 A L_{\mathrm{CV}} = a_p \rho_1 A L_{\mathrm{CV}} \tag{10}$$

Therefore,

$$\frac{\partial}{\partial t}\int_{\mathrm{CV}} \rho u \,\mathrm{d}V \approx 2 a_p \rho_1 A L_{\mathrm{CV}} \tag{11}$$

Assuming the projectile reference frame accelerates uniformly, the second integral in the momentum equation (2) can be evaluated as

$$\int_{\mathrm{CV}} a_p \rho \,\mathrm{d}V = m_g a_p \approx a_p \rho_1 A L_{\mathrm{CV}} \tag{12}$$

When the thrust is expressed in terms of the projectile acceleration that is, $F = m_p a_p$, the momentum equation becomes

$$a_p \rho_1 A L_{\mathrm{CV}} + A\left(P_2 + \rho_2 u_2^2\right) - A\left(P_1 + \rho_1 u_1^2\right) - m_p a_p = 0 \tag{13}$$

The net unsteady term $a_p \rho_1 A L_{\mathrm{CV}}$ has the opposite algebraic sense as the net thrust term $m_p a_p$; the indication of the opposite signs is that some of the available momentum in the flow (as indicated by the convective terms) is being expended in accelerating the gas accumulating in the control volume, rather than being used to accelerate the projectile.

In the energy equation (3), the first integral term is the accumulation of energy within the control volume, and the second integral is the work resulting from the acceleration of the projectile-fixed coordinate system. For typical operating conditions, $e_2 \approx u_1^2$, and if this is taken as a maximum value for the internal energy, the accumulation term can be evaluated as[6]

$$\frac{\partial}{\partial t}\int_{\mathrm{CV}} \rho\left(e + \frac{u^2}{2}\right)\mathrm{d}V \approx \frac{\partial}{\partial t}\int_{\mathrm{CV}} \frac{3}{2}u_1^2 \rho \,\mathrm{d}V \approx \frac{9}{2} a_p \rho_1 u_1 A L_{\mathrm{CV}} \tag{14}$$

The acceleration work term can be evaluated as

$$\int_{\mathrm{CV}} u a_p \rho \,\mathrm{d}V \approx a_p \rho_1 u_1 A L_{\mathrm{CV}} \tag{15}$$

The energy equation therefore becomes

$$\tfrac{7}{2} a_p \rho_1 u_1 A L_{\mathrm{CV}} + A\rho_2 u_2 \left(h_2 + u_2^2/2\right) - A\rho_1 u_1 \left(h_1 + u_1^2/2 + \Delta q\right) = 0 \tag{16}$$

With the conservation equations expressed solely in algebraic terms, an expression for the acceleration can be determined in terms of known quantities, given an equation of state and the thermally choked state at station 2. For this analysis, the ideal-gas equation of state will be assumed; it will also be assumed, for simplicity, that the gas is calorically perfect with constant specific heat capacity (i.e., $h_1 = C_p T_1$ and $h_2 = C_p T_2$). These assumptions allow the expressions $M_1\sqrt{(\gamma R T_1)}$ and $\sqrt{(\gamma R T_2)}$ to be substituted for the velocities u_1 and u_2, respectively. Consequently, the conservation equations are reduced to

$$\frac{P_1 a_p A L_{\mathrm{CV}}}{M_1\sqrt{\gamma R^3 T_1^3}} + P_2 A\sqrt{\frac{\gamma}{RT_2}} - P_1 A M_1\sqrt{\frac{\gamma}{RT_1}} = 0 \tag{17}$$

$$\frac{P_1 a_p A L_{\mathrm{CV}}}{RT_1} + A P_2(1+\gamma) - A P_1\left(1+\gamma M_1^2\right) - m_p a_p = 0 \tag{18}$$

$$\frac{\frac{7}{2} P_1 a_p A L_{\mathrm{CV}} M_1}{\sqrt{\gamma RT_1}} + \frac{\gamma+1}{2(\gamma-1)} A P_2\sqrt{\gamma RT_2} - A P_1 M_1 \frac{\sqrt{\gamma RT_1}}{\gamma-1}\left(1 + \frac{\gamma-1}{2}M_1^2 + Q\right) = 0 \tag{19}$$

Solving the reduced momentum equation (18) for the unknown P_2,

$$P_2 = \frac{m_p a_p + A P_1\left(1+\gamma M_1^2\right) - P_1 a_p A L_{\mathrm{CV}}/RT_1}{A(\gamma+1)} \tag{20}$$

Substituting into the reduced continuity equation (17),

$$\frac{P_1 a_p A L_{\mathrm{CV}}}{M_1\sqrt{\gamma R^3 T_1^3}} + \frac{\left(m_p a_p + A P_1\left(1+\gamma M_1^2\right) - P_1 a_p A L_{\mathrm{CV}}/RT_1\right)}{(\gamma+1)} \times \sqrt{\frac{\gamma}{RT_2}} - P_1 A M_1\sqrt{\frac{\gamma}{RT_1}} = 0 \tag{21}$$

Solving the above equation (21) for the unknown T_2,

$$T_2 = \frac{\gamma\left(m_p a_p + A P_1\left(1+\gamma M_1^2\right) - P_1 a_p A L_{\mathrm{CV}}/RT_1\right)^2}{R(\gamma+1)^2\left(P_1 A M_1\sqrt{\gamma/RT_1} - P_1 a_p A L_{\mathrm{CV}}\big/M_1\sqrt{\gamma R^3 T_1^3}\right)^2} \tag{22}$$

Substituting the expressions for P_2 and T_2 into the reduced energy equation (19),

$$\frac{\frac{7}{2} P_1 a_p A L_{\mathrm{CV}} M_1}{\sqrt{\gamma RT_1}} + \frac{\gamma\left(m_p a_p + A P_1\left(1+\gamma M_1^2\right) - P_1 a_p A L_{\mathrm{CV}}/RT_1\right)^2}{2(\gamma+1)(\gamma-1)\left(P_1 A M_1\sqrt{\gamma/RT_1} - P_1 a_p A L_{\mathrm{CV}}\big/M_1\sqrt{\gamma R^3 T_1^3}\right)} - A P_1 M_1\frac{\sqrt{\gamma RT_1}}{\gamma-1}\left(1 + \frac{\gamma-1}{2}M_1^2 + Q\right) = 0 \tag{23}$$

The result is an algebraically implicit expression for determining the dependent variable a_p as a function of the projectile Mach number M_1. All other parameters in Eq. (23) can be specified a priori either directly (the undisturbed propellant pressure P_1 and temperature T_1, the tube cross-sectional area A, and the projectile mass m_p) or indirectly through the propellant composition (the gas constant R, the specific heat ratio γ, and the heat-release parameter Q). Previous experiments have shown that the combustion during thermally choked ram accelerator operation at Mach 3.7 is completed within approximately one projectile length behind the projectile base.[6] The length of the combustion zone is expected, however, to decrease with increasing Mach number because the increasing static temperature of the flow enhances the chemical kinetic rates. For the purpose of concisely illustrating the effects of projectile acceleration on the thrust of the ram accelerator, however, it is assumed in this analysis that the control volume length is constant and equal to $L_{\mathrm{CV}} = 2L_p$: The influence of Mach number on the length of the combustion zone length is still under investigation.

To check the validity of Eq. (23), the thrust ($F = m_p a_p$) is determined for the limit of small acceleration:

$$F = A P_1\left(M_1\sqrt{2(\gamma+1)\left\{1 + [(\gamma-1)/2]M_1^2 + Q\right\}} - \left(1+\gamma M_1^2\right)\right) \tag{24}$$

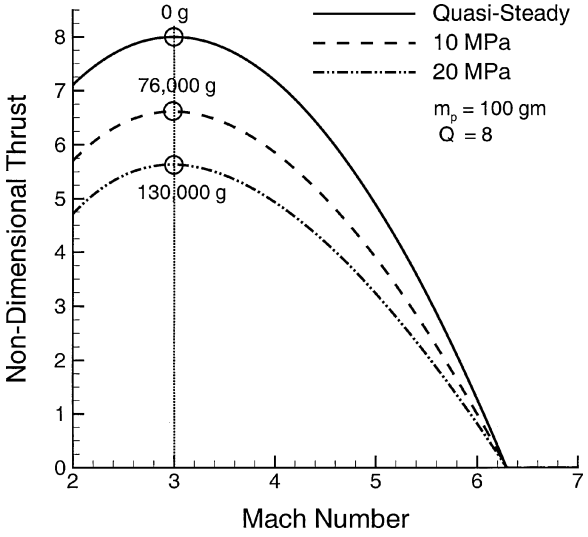

Fig. 2 Thrust coefficient variation with fill pressure for the unsteady flow model of the thermally choked ram accelerator.

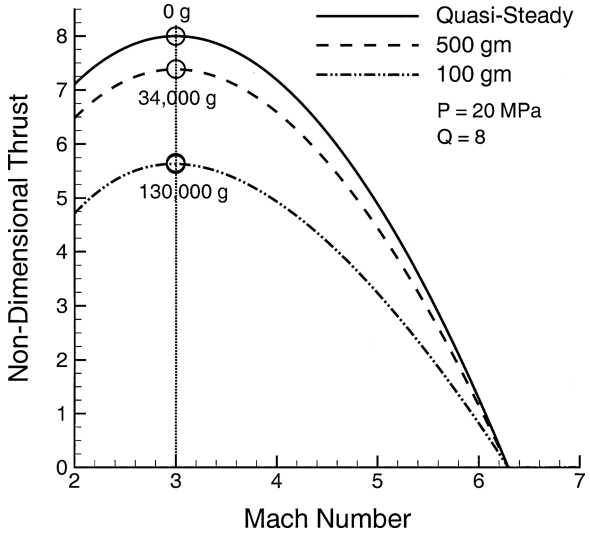

Fig. 3 Thrust coefficient variation with projectile mass for the unsteady flow model of the thermally choked ram accelerator.

which is the thrust solution for the quasi-steady control volume model.[1] The same result is obtained in the limit of small fill pressure and in the limit of infinite projectile mass. Similarly, if an acceleration of zero (i.e., zero thrust) is prescribed and the unsteady thrust equation solved for the projectile Mach number,

$$M_1^2 = [1 + (\gamma + 1)Q] + \sqrt{[1 + (\gamma + 1)Q]^2 - 1} \qquad (25)$$

which is identical to that of a one-dimensional Chapman–Jouguet detonation wave propagating through the propellant. This is the same result obtained by the quasi-steady control volume model.[1] Thus, both the unsteady and quasi-steady models predict that the maximum velocity to which a projectile can be accelerated in the thermally choked ram accelerator propulsive mode is that of the CJ detonation wave of the propellant, which is to be expected because the thrust, and hence acceleration, becomes vanishingly small as the CJ speed is approached.

As fill pressure increases, the unsteady terms of the thrust equation become larger and have the effect of reducing the thrust coefficient obtained from quasi-steady modeling. This effect on projectile acceleration is demonstrated by the plots of thrust coefficient vs Mach number presented in Fig. 2. These thrust coefficient curves were determined from the unsteady thrust equation using the following parameters: $Q = 8$, $\gamma = 1.35$, $m_p = 100$ g, $T_1 = 295$ K, $R = 330$ J/kg-K, $L_{CV} = 22.86$ cm, and $A = 11.4$ cm^2, which are values similar to those that occur in typical high-pressure ram accelerator experiments in the 38-mm-bore facility. All of the thrust coefficient curves converge to zero at the same Mach number because the zero thrust condition for thermally choked flow at a given pressure is always that of a CJ detonation wave in the propellant. The Mach-number profile of the quasi-steady thrust coefficient ($a_p = 0$) is also shown in Fig. 2, and the corresponding peak accelerations for each of the thrust coefficient curves are indicated. Although the acceleration obtained increases with propellant fill pressure, as expected, the associated thrust coefficient decreases with increasing fill pressure. The implication of this decrease is that when including the unsteady effects of high acceleration on ram accelerator operation the actual thrust will increase more slowly with pressure than the direct proportional scaling predicted by the quasi-steady model.

The unsteady one-dimensional modeling indicates that as the mass of gas within the control volume becomes nonnegligible compared to the mass of the projectile, less of the net momentum is available to accelerate the projectile because more is absorbed in accelerating the gas inside the control volume. Thus, it is expected that as the projectile mass decreases the thrust coefficient should decrease as well. This effect is shown in Fig. 3. The unsteady thrust coefficient curves in this figure were determined from Eq. (23) using the same propellant thermodynamic parameters as in the preceding example, but with the pressure fixed at 20 MPa and using different values of projectile mass as a parameter. The quasi-steady thrust determined for these thermodynamic parameters is also shown for comparison. As the projectile mass is decreased, the acceleration for a given Mach number increases, as expected. The associated thrust coefficient, however, decreases with decreasing mass; thus, the acceleration scales up with decreasing mass at a rate less than that obtained from inverse proportional scaling. When the projectile mass is lowered to a value similar to that used in high-pressure experiments ($\sim$100 g), the thrust coefficient is substantially lower than that of the quasi-steady model.

The discussion of the unsteady model has not included the real-gas effects on high-pressure reactants and combustion products. Although it would be highly desirable to generate an equation similar to Eq. (23), which incorporates a real-gas equation of state, a closed-form solution for the acceleration under unsteady flow conditions is not possible; however, real-gas effects on the unsteady thrust can be accounted for by making appropriate substitutions of real-gas values of operating parameters in the governing equations. An analysis of the sensitivity of the unsteady model to heat release, control volume pressure ratio, and acoustic speed at the thermal choking point is presented in the Appendix. The result of this theoretical analysis is that the thrust coefficient is considerably more sensitive to the influence of increased heat release as a result of real-gas effects than to the latter two parameters, at all values of the projectile Mach number.[16] Therefore, for purposes of further discussion, real-gas effects are incorporated into the unsteady model by using the Mach-number variation of heat-release parameter Q calculated with the Boltzmann equation of state.

Experimental Facility

The ram accelerator facility at the University of Washington is capable of being operated with propellant fill pressures up to 20 MPa. Brief descriptions of the high-pressure portion of the launch tube and the projectile configuration used in the experiments are provided in this section. References 13, 15, and 16 provide the details of the light-gas gun prelauncher, propellant filling system, and other major system components.

Ram Accelerator Tubes and Instrumentation

The first 4 m of the ram accelerator test section, shown in Fig. 4, consists of two 1-m-long and one 2-m-long high-pressure tubes, with an outer diameter of 152 mm and an inner diameter of 38 mm, connected together using bolted flange joints.[16] The high-pressure tubes are manufactured from AISI 4340 steel and are designed for a maximum static load of 1000 MPa. The remaining 12 m of the test section is comprised of six low-pressure tubes manufactured

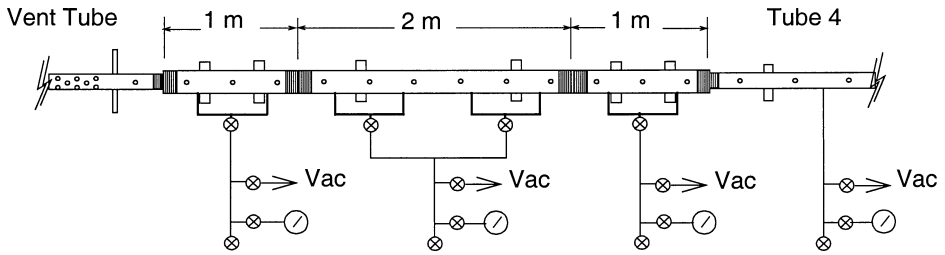

Fig. 4 High-pressure test section of the 38-mm bore ram accelerator facility.

from AISI 4140 steel, each 2 m in length, with outer diameters of 102 mm. These tubes are connected with threaded collars and are designed to withstand a static load of up to 550 MPa. The two parts of the test section are connected using a bolted flange joint containing a transition piece to properly join the two different tube designs.

Each 1-m-long tube (Fig. 4) has three instrument stations with diametrically opposed ports; the 2-m-long tube has six pairs of ports. These stations are spaced along the tubes at 333-mm intervals. The first instrument station in the high-pressure test section is 167 mm from the entrance diaphragm, and the last station is located 167 mm from the section's exit and 396 mm from the first instrument port in the low-pressure part of the test section. In the latter, the instrument stations are spaced 400 mm apart. The instrument ports accommodate PCB model A119A11 and A119A12 piezoelectric pressure transducers (550 and 800 MPa maximum pressure range, respectively) and electromagnetic transducers.

All of the tubes in the high-pressure test section have two gas fill ports per meter of length, as shown in Fig. 4. These fill ports are isolated from the fill lines by air-actuated Snotrik valves (300 MPa rated), which protect the gas handling system from the extreme pressure pulses generated in the experiments. The low-pressure tubes in the test section have fill ports midway along their lengths. Mylar diaphragms can be inserted between any pair of adjacent tubes, enabling multiple stages of different propellants to be used. Any tubes not filled with a propellant are evacuated.

Projectile and Obturator

The four-fin configuration of the one-piece projectiles used in this investigation is shown in Fig. 5a. These projectiles are manufactured from titanium 6Al-6V-2Sn alloy and feature a fin span of 38 mm, throat diameter of 23 mm (point of maximum projectile cross-sectional area, as indicated in Fig. 1), nose cone angle of 12.5 deg, and a fin rake angle of 20 deg. They have a 14 mm diameter cavity that is center-drilled from the rear of the projectile. A neodymium magnet is inserted into this cavity and held in place by a threaded magnesium plug. The remainder of the cavity is left open to reduce the overall mass of the projectile. The fin leading edges are knife-edged at a 15-deg angle to their centerlines in order to reduce the strength of the shock waves generated by the fins near the projectile throat. The afterbody length is either 64 or 76 mm, which results in projectile masses of 106 or 118 g, respectively. The use of lower mass projectiles is necessary to increase the entrance velocity to the test section.

The obturator, shown in Fig. 5b, is placed behind the projectile base to prevent gas blow-by from the light gas gun and to drive a normal shock wave onto the projectile afterbody upon entrance to the test section. The obturator is a single piece manufactured from polycarbonate plastic and has a mass of 18 g. It is initially attached to the projectile with cyanoacrylate adhesive to keep it from separating during the process of loading the light gas gun.

Experimental Results

Various aspects of the experimental data from this high pressure investigation have been presented in Refs. 13, 15, 19, and 20; whereas a complete compilation of the data is presented in Ref. 16. A summary of the phenomena observed during the starting process and

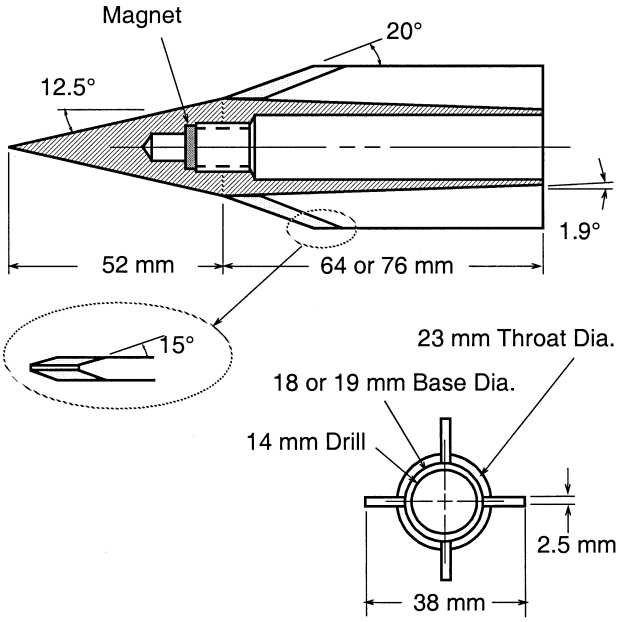

Fig. 5a One-piece titanium projectile design.

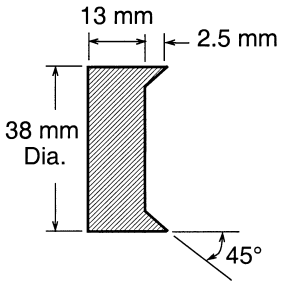

Fig. 5b Solid polycarbonate obturator.

the results of high pressure experiments pertinent to understanding the unsteady effects of projectile acceleration are presented in this section.

Starting Process of the Thermally Chocked Ram Accelerator

The starting process in the ram accelerator encompasses the phenomena associated with launching the subcaliber projectile and tube-occluding obturator by means of a light-gas gun to the entrance of the ram accelerator test section, and the establishment of the thermally choked ram accelerator flowfield.[2,3] Propellant ignition occurs as a result of the complex interactions of the launch-generated shock waves in the residual air in the launch tube with the projectile, the obturator, and the diaphragm at the entrance to the test section.[21–23] After driving a normal shock wave onto the rear body of the projectile, the obturator then quickly recedes and ceases to influence the flowfield after the projectile has traveled for about 1 m beyond the test-section entrance.[24–26] The ram accelerator is successfully started once supersonic flow is established behind the

projectile throat and the normal shock wave is stabilized on the rear body by thermal choking of the flow behind the projectile, as shown in Fig. 1.

Under certain conditions a prolonged delay in the combustion stabilization process occurs, whereby the flow remains supersonic relative to the projectile throat and the projectile is weakly accelerated. Ultimately, the flow becomes thermally choked, and the acceleration increases dramatically. This weak acceleration phase of the starting process is referred to as a "delayed start." In experiments using short test sections, for example, 1 m, there might not be sufficient travel distance for the projectile to establish thermal choking and achieve a successful start; however, the delayed start does indicate that the conditions necessary for a successful start, other than thermal choking, are satisfied.[15]

When the necessary conditions for ram accelerator starting (prompt or delayed) are not met, the projectile decelerates. If either the entrance velocity to the test section is too low or there is substantial heat release ahead of the projectile throat, then the flow chokes at the throat, and a strong normal shock wave is driven ahead of the projectile. This result, when caused by these phenomena, is referred to as a sonic diffuser unstart. If the normal shock wave is pushed ahead of the projectile at some time after supersonic flow is established behind its throat, thrust ceases, and the resulting failure is referred to as a wave unstart. Some factors that produce wave unstarts include too much heat release from the propellant, too much flow occlusion by the obturator, and/or excessive obturator mass. The outcome of a ram accelerator start attempt is readily determined from tube wall pressure data and the velocity–distance profile of the projectile.[23]

Starting Process of the Ram Accelerator at Elevated Pressure

High-pressure experiments previously conducted with the 38-mm-bore facility in 15-MPa propellants showed that titanium projectiles with a throat diameter of 25 mm (flow throat to tube diameter area ratio of 0.57), afterbody length of 51 mm, and mass of 108 g could be ram accelerated in propellants with a wide range of methane/oxygen/nitrogen compositions for distances up to 3 m before a wave unstart caused acceleration to cease.[13,15,19] Invariably, the projectiles experienced a delayed start in the first meter of the test section and accelerated at rates much lower than expected for quasi-steady thermally choked operation. After the first meter, the acceleration increased substantially, but it was still overpredicted by the quasi-steady thrust model using the Boltzmann equation of state.[13]

Additional experiments conducted in 20-MPa propellants demonstrated that a reduction of throat diameter was necessary in order for the ram accelerator process to be initiated at entrance velocities as low as 1220 m/s (Refs. 15 and 20). This result led to a new projectile design for 20-MPa operation in which the throat diameter was reduced to 23 mm and the afterbody length increased to 76 mm, as shown in Fig. 5a. The results of 15–20-MPa experiments using these projectiles are compared with theory in what follows.

Four-Meter-Long 15-MPa Experiment

The velocity–distance data from an experiment using $2.6CH_4 + 2O_2 + 9.2N_2$ propellant at a fill pressure of 15 MPa are shown in Fig. 6. The titanium projectile had an afterbody length of 76 mm and overall mass of 118 g (Fig. 5a). The uncertainty in determining the velocity from time-distance data is approximately 2.5%, as indicated by the vertical error bars. Ram accelerator operation was initiated at an entrance velocity of 1190 m/s, and the projectile was accelerated continuously throughout the 4-m-long test section. The experimental data show that the projectile experienced relatively weak acceleration over the first meter of the stage, averaging ~9000 g over this distance, indicating a delayed starting process. Subsequently, the projectile velocity–distance curve significantly steepened as the acceleration increased by a factor of ~3. The average acceleration over the last 3 m of the test section was 31,300 g, and the exit velocity of the projectile was 1860 m/s.

The velocity–distance profiles predicted by the quasi-steady and unsteady models are also shown in Fig. 6 for comparison. These

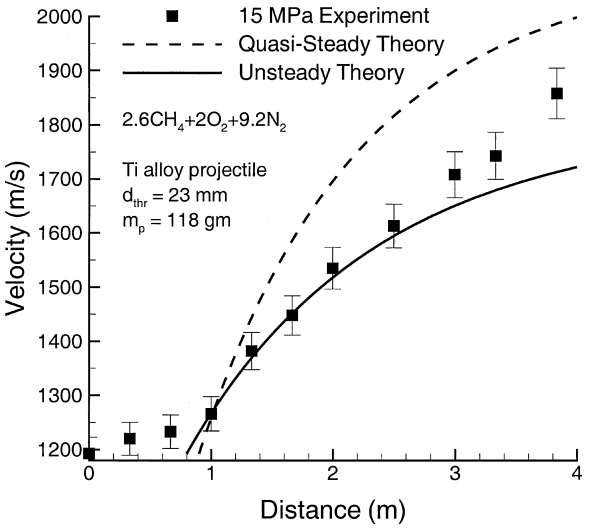

Fig. 6 Velocity–distance data from 15-MPa experiment in a 4-m-long test section.

were determined by integrating the equation of motion, using the theoretical results for the net thrust. The unsteady velocity–distance curve was determined at increments of distance evenly spaced on a logarithmic scale, so as to minimize computational error at low velocities where the acceleration rates are theoretically greatest, and to reduce the number of computational iterations required at high velocities where the acceleration rates are relatively small. Because the primary interest is to compare the experimental and theoretical thrust at a given velocity, the theoretical velocity–distance curves are positioned so that they pass through the experimental velocity datum point located 1 m after the entrance to the test section, at which point thermal choking is presumed to be fully established.

The relatively low acceleration at the entrance to the test section, evident in Fig. 6, suggests that the ram accelerator is not thermally choked over the first meter; however, the experimental data suggest that thermal choking likely occurs farther down the tube as indicated by the better theoretical and experimental agreement observed over the final 3 m of the test section. The delayed-start effect has been observed in prior 15-MPa experiments[13,15,19] and at other ram accelerator facilities using fill pressures of 3–4.5 MPa (Refs. 27–29). This effect is magnified by increased propellant fill pressure. It has not yet been determined whether the weak acceleration during a delayed start is caused by the effects of the unsteady flowfield, rapid deceleration of the obturator, an increase in the induction time of the propellant at high pressure, or a combination of these and/or other causes. The phenomenon is still under investigation.

It is also apparent from the curves in Fig. 6 that the quasi-steady control volume model consistently overpredicts the experimental velocity–distance data in the thermally choked operating mode, whereas the unsteady velocity–distance calculation provides significantly improved agreement with experiment. Consequently, the more appropriate theory for predicting ram accelerator thrust performance at high pressures is the unsteady model, and thus only its results are presented with the experimental data discussed next.

Two-Stage Experiments

Initial attempts to start the 118-g projectile directly in 20-MPa propellants were not successful at entrance velocities of ~1200 m/s (Ref. 20); thus, a two-stage configuration was used in which the projectile was first started in 15-MPa propellant before it entered a second stage containing propellant at 20 MPa. This procedure was successful in decoupling the effects of the starting process from the ram accelerator operating process at 20 MPa. In these starting- decoupled experiments, the test section consisted of a 1-m-long stage of $2.6CH_4 + 2O_2 + 9.2N_2$ propellant at 15 MPa, followed by a 3-m-long stage of the same propellant at 20 MPa. The velocity–distance data from two of these experiments, having a 20 m/s difference in entrance velocity, are shown in Fig. 7. Because

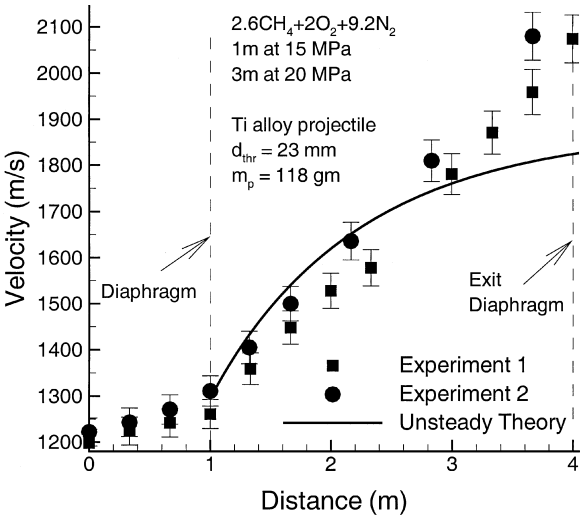

Fig. 7 Velocity–distance data for 20-MPa two-stage experiments using titanium projectiles.

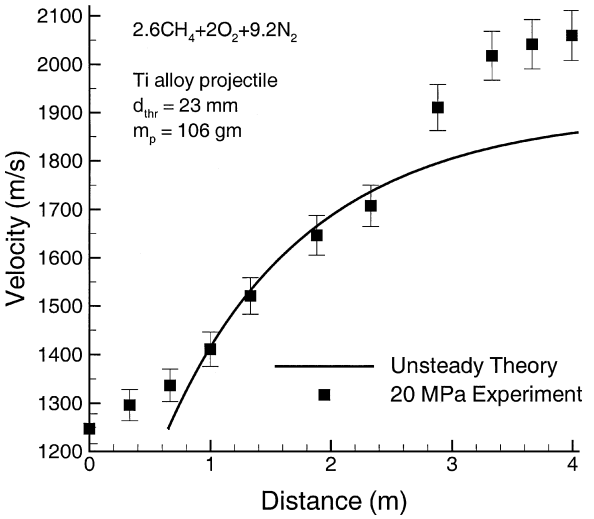

Fig. 8 Velocity–distance data from 20-MPa experiment in a 4-m-long test section.

the variation between the corresponding unsteady theory curves is minor, only the theoretical results for experiment 2 are plotted for comparison.

The projectiles entered the 15-MPa stage at a velocity of ∼1200 m/s, successfully initiated ram accelerator operation, reached a velocity of 1260–1310 m/s at the entrance to the 20-MPa stage, and then continuously accelerated through the last 3 m of the test section (Fig. 7) to reach peak velocities of 2070–2100 m/s. Both projectiles experienced weak acceleration (8000–12,000 g) in the starting stage, indicative of a delayed start. At the entrance to the second stage, the projectile thrust increased by a factor of ∼4, which is in good agreement with the unsteady theoretical prediction for these conditions. After accelerating a distance of ∼1.5 m in the second stage, the projectile thrust begins to significantly exceed that of theory. This enhanced thrust at the end of the second stage indicates that the has ceased to be thermally choked behind the projectile. The average acceleration over the last 3 m of these experiments of 46,000 g, whereas the theory predicts an average of 28,000 g.

Four-Meter Long 20-MPa Experiment

Because operation at 20 MPa was successfully achieved once the 15-MPa propellant had accelerated the projectile to a velocity greater than 1250 m/s, an experiment was conducted to attempt starting directly in 20 MPa at a comparable entrance velocity. A titanium projectile with its afterbody length shortened to 64 mm (which reduced its mass to 106 g to permit a higher entrance velocity) was launched into a 4-m-long test section of $2.6CH_4 + 2O_2 + 9.2N_2$ propellant at 20-MPa fill pressure. The velocity–distance data from this experiment are shown in Fig. 8. The projectile entered the test section at ∼1250 m/s and accelerated continuously through the test section to a peak velocity of 2060 m/s. Just like in the prior experiments, the projectile experienced a delayed start over the first meter of the test section, but the lower acceleration (average of 22,000 g over the first meter) was not as pronounced as before.

The velocity–distance profile predicted for the unsteady ram accelerator thermally choked propulsive mode is also shown in Fig. 8, where again the theoretical curve is positioned so that it passes through the experimental velocity datum point located 1 m from the entrance to the test section, where thermally choking is presumed to be fully established. The velocity–distance profiles of the unsteady model and experiment are in good agreement for the 1- to 2.5-m portion of the test section; afterwards, the projectile thrust is substantially higher than theory. The average acceleration of the projectile in this region of operation is ∼48,000 g. The projectile acceleration is again greater than that predicted by the unsteady theoretical model in the last meter or so of the test section; however, the thrust tapers off before the projectile exits. The average acceleration of the projectile is ∼38,000 g over the last 3 meters of the test section, which is ∼20% lower than that observed in prior two-stage experiments, even the projectile mass was reduced 10%.

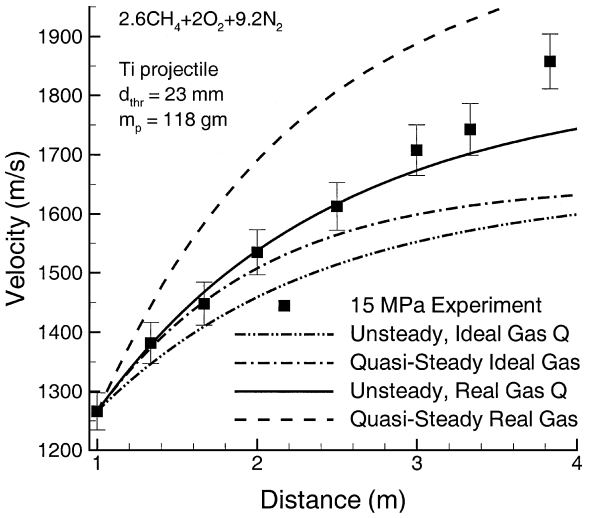

Fig. 9 Velocity–distance profiles for unsteady and quasi-steady thrust models.

Discussion of Results

The velocity–distance curves for thermally choked ram accelerator operation predicted by the quasi-steady and unsteady thrust models for the last 3 m of the 15-MPa experiment (Fig. 6) are shown in Fig. 9. The corresponding experimental velocity–distance data are also plotted. The quasi-steady curves were calculated using both the ideal-gas and Boltzmann equations of state. The two unsteady curves were determined by using two different heat-release vs Mach-number ($Q - M$) variation profiles; one used the $Q - M$ profile indicated by the ideal-gas equation of state and the other used that which resulted from applying the Boltzmann equation of state. Based on the sensitivity analysis presented in the Appendix, this approach enables real-gas effects to be incorporated with reasonable accuracy into the unsteady model.

It is evident that the thrust coefficient of the unsteady model is significantly reduced because of the much smaller velocity gain it predicts over a given distance compared to the quasi-steady model. The experimental data, however, indicate greater velocity gain with distance than either of the models using the ideal-gas $Q - M$ variation profile. On the other hand, the quasi-steady model using the heat release predicted with the Boltzmann equation of state predicts

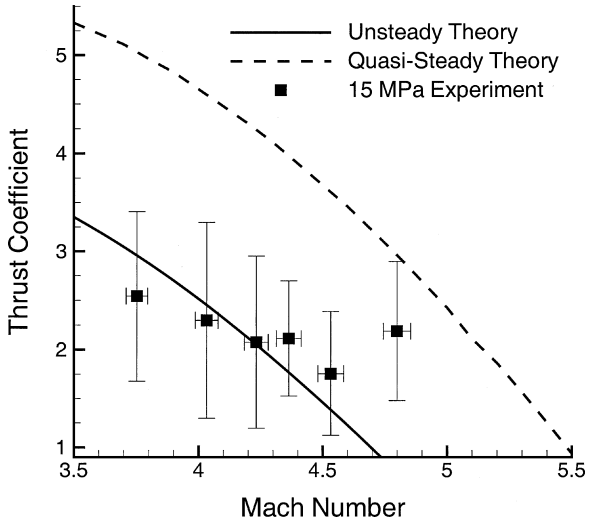

Fig. 10 Thrust coefficient Mach-number profiles for unsteady and quasi-steady thrust models.

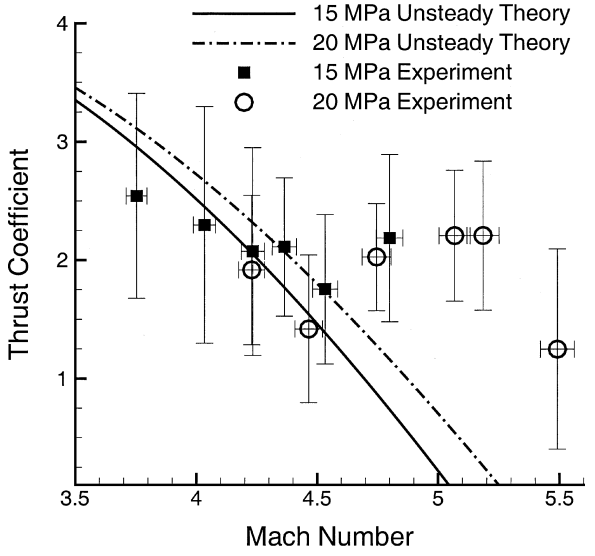

Fig. 11 Thrust coefficient Mach-number profiles for 15- and 20-MPa experiments, compared with the unsteady flow model.

a much greater velocity gain with distance than is obtained in the experiment. The unsteady model using the real-gas $Q - M$ variation profile gives the best agreement with experimental results.

The magnitude of the differences between steady and unsteady modeling of thermally choked ram accelerator performance is more apparent when comparing the thrust coefficient vs Mach-number profiles for the aforementioned experiment, as shown in Fig. 10. In this figure, the net effect of unsteady and real-gas effects upon the thrust coefficient is compared with the experiment at 15 MPa. The projectile acceleration is determined by double-differentiating time–distance data from instrumentation stations that are separated by 1.0–1.7 m, which results in maximum experimental thrust coefficient uncertainties of ~70%, as indicated by the vertical error bars. This data-reduction procedure has been found to adequately highlight the general trends in ram accelerator thrust vs Mach-number behavior in lieu of averaging the results of multiple experiments to reduce experimental uncertainty. (Experimental results are very repeatable as indicated by data in Fig. 7; thus, the influence of small changes in control variables is typically investigated more often than the repeatability of performance under a specific set of conditions.) Ultimately, onboard acceleration measurements and/or direct in-bore velocity tracking will enable a more accurate measurement of the experimental thrust coefficient.

When the $Q - M$ variation determined with the Boltzmann equation of state is utilized, the unsteady thrust model prediction of the thrust coefficient vs Mach-number behavior is in very good agreement with the experimental conditions modeled, whereas the quasi-steady calculation that incorporates these real-gas effects predicts a much greater thrust coefficient than observed in the experiment. Consequently, the velocity–distance profiles determined by integrating the unsteady thrust coefficient model, which incorporates the real-gas $Q - M$ variation, are in very good agreement with experiment at velocities below 75% CJ detonation speed, as shown in Figs. 6–9.

The thrust coefficient data for the 4-m-long experiments at 15 and 20 MPa are presented in Fig. 11, along with the corresponding unsteady theoretical modeling results using the $Q - M$ variations predicted with the Boltzmann equation of state. Over the Mach-number range shown, the theoretical thrust coefficient at 20 MPa exceeds that at 15 MPa primarily because the heat release is greater at the higher fill pressure; however, this difference in thrust also depends to some degree on the length of control volume assumed in the unsteady modeling. The significance of the length of control volume on this model of ram accelerator performance is being investigated.

The amplitude and trend with increasing Mach number of the thrust coefficient data from the 20-MPa experiment are practically the same as those of the 15-MPa experiment up to Mach 4.5, after which the experimental thrust levels remain much higher than those predicted by the unsteady model (Fig. 11). The deviation of the experimental data from the trend of decreasing thrust at higher Mach numbers is consistent with results at lower pressures (2.5–5.0 MPa) in a wide range of propellants.[30–32] Numerical modeling has shown that this behavior might be caused, in part, by the combustion process moving up onto the projectile afterbody as the induction time decreases with increasing temperature.[7] Alternatively, the aerothermal heating of the projectile can be intense enough for the titanium alloy to begin to react with the propellant oxidizer, a phenomenon that has been previously observed and exploited with aluminum and magnesium projectiles.[33,34] Even though this anomalous thrust behavior, in the context of the model for thermally choked ram accelerator operation, is not yet well understood, it is repeatable and has been observed in all experimental facilities.[24,27–34]

Previous experiments have shown that the afterbody length of the projectile is a key factor in determining how far it will accelerate in the high-pressure test section.[15,20] Thus it seems likely that the lower average acceleration in the last 3 meters of the test section observed with the lower mass projectile in 20-MPa propellant is due to the shortened body. The impact of projectile geometry on high-pressure operation is still under investigation.

Conclusions

Experiments in the 38-mm-bore ram accelerator facility have shown the feasibility of continuously accelerating titanium projectiles in propellants at fill pressures up to 20 MPa, the highest pressure at which ram accelerator operation has been demonstrated to date. Smaller projectile throat diameter (23 mm) and higher entrance velocity (1250 m/s) were required to initiate ram accelerator operation at this propellant fill pressure than at lower pressures. After a delayed start in the first meter of the test section, thermal choking seems to be established as evidenced by a sudden increase in acceleration by a factor of 3 or more. The projectile acceleration then steadily decreases as it gains velocity until its Mach number approaches ~4.5, after which the acceleration significantly exceeds that predicted for thermally choked ram accelerator operation. Total velocity gains of 900 m/s and average accelerations of 42,000–46,000 g have been demonstrated with 106–118 g projectiles in 20-MPa propellant in a 4-m-long test section.

Because the quasi-steady one-dimensional model overpredicts the experimental acceleration, a revision was made to the model to include the unsteady terms in the conservation equations. The new unsteady ram accelerator thrust model indicates that the mass of propellant in the control volume has a significant effect on the body forces experienced by the system when the propellant mass is of the same order as the projectile mass. The Mach-number dependence

predicted by the unsteady model of the thrust coefficient deviates considerably from that predicted by the quasi-steady model when the fill pressure is increased, a result consistent with experimental observations. When the unsteady control volume model is applied with the heat-release behavior obtained from the Boltzmann real-gas equation of state, the theoretical velocity–distance profile has significantly better agreement with experimental results during thermally choked operation.

Appendix: Sensitivity of Unsteady Thrust Model to Real-Gas Effects

Bundy et al.[13] have shown that the thrust coefficient is augmented by increases in propellant heat release Q, in the pressure ratio, P_2/P_1, between the thermal choking plane and freestream conditions and in the acoustic speed at the thermal choking plane c_2. Each of these parameters has a dependency on in-tube Mach-number, which varies when a real-gas is used rather than the ideal-gas equation of state. Further, each of these parameters is interdependent on each of the others. If the real-gas Mach-number profile of the parameter that most influences the thrust coefficient is used in Eq. (23) real-gas effects can be incorporated into the unsteady thrust model while retaining a closed-form solution.

To determine which parameter has the greatest influence on the thrust coefficient when a real-gas equation of state is used, Eqs. (20), (22), and (23) are arranged to express the acceleration in terms of P_2/P_1, c_2, and Q:

$$\frac{P_2}{P_1} = \frac{m_p a_p/P_1 + A\left(1+\gamma M_1^2\right) - AL_{\mathrm{CV}} a_p/RT_1}{A(\gamma+1)} \tag{A1}$$

$$c_2 = \frac{\gamma\left[m_p a_p/P_1 + A\left(1+\gamma M_1^2\right) - AL_{\mathrm{CV}} a_p/RT_1\right]}{(\gamma+1)\left(AM_1\sqrt{\gamma/RT_1} - Aa_p L_{\mathrm{CV}}\Big/ M_1\sqrt{\gamma R^3 T_1^3}\right)} \tag{A2}$$

$$\frac{\frac{7}{2}AL_{\mathrm{CV}} a_p M_1}{\sqrt{\gamma RT_1}} + \frac{\gamma+1}{2(\gamma-1)}AC_2\left(\frac{P_2}{P_1}\right) - AM_1\frac{\sqrt{\gamma RT_1}}{\gamma-1}\left(1+\frac{\gamma-1}{2}M_1^2+Q\right) = 0 \tag{A3}$$

Defining $P_{\mathrm{rat}} = P_2/P_1$, Eq. (A3) is then differentiated with respect to Q:

$$\frac{\frac{7}{2}AL_{\mathrm{CV}} M_1}{\sqrt{\gamma RT_1}}\left(\frac{\mathrm{d}a_p}{\mathrm{d}Q}\right) + \frac{\gamma+1}{2(\gamma-1)}A\left[P_{\mathrm{rat}}\left(\frac{\mathrm{d}c_2}{\mathrm{d}Q}\right) + c_2\left(\frac{\mathrm{d}P_{\mathrm{rat}}}{\mathrm{d}Q}\right)\right] - AM_1\frac{\sqrt{\gamma RT_1}}{\gamma-1} = 0 \tag{A4}$$

where $\mathrm{d}P_{\mathrm{rat}}/\mathrm{d}Q$ and $\mathrm{d}c_2/\mathrm{d}Q$ are determined as implicit functions of $\mathrm{d}a_p/\mathrm{d}Q$ from Eqs. (A1) and (A2), respectively. Equation (A4) is then solved for $\mathrm{d}a_p/\mathrm{d}Q$. In similar fashion, Eq. (A3) is differentiated with respect to P_{rat} and c_2:

$$\frac{\frac{7}{2}AL_{\mathrm{CV}} M_1}{\sqrt{\gamma RT_1}}\left(\frac{\mathrm{d}a_p}{\mathrm{d}P_{\mathrm{rat}}}\right) + \frac{\gamma+1}{2(\gamma-1)}A\left[P_{\mathrm{rat}}\left(\frac{\mathrm{d}c_2}{\mathrm{d}P_{\mathrm{rat}}}\right) + c_2\right] - AM_1\frac{\sqrt{\gamma RT_1}}{\gamma-1}\left(\frac{\mathrm{d}Q}{\mathrm{d}P_{\mathrm{rat}}}\right) = 0 \tag{A5}$$

$$\frac{\frac{7}{2}AL_{\mathrm{CV}} M_1}{\sqrt{\gamma RT_1}}\left(\frac{\mathrm{d}a_p}{\mathrm{d}c_2}\right) + \frac{\gamma+1}{2(\gamma-1)}A\left[P_{\mathrm{rat}} + c_2\left(\frac{\mathrm{d}P_{\mathrm{rat}}}{\mathrm{d}c_2}\right)\right] - AM_1\frac{\sqrt{\gamma RT_1}}{\gamma-1}\left(\frac{\mathrm{d}Q}{\mathrm{d}c_2}\right) = 0 \tag{A6}$$

where $\mathrm{d}Q/\mathrm{d}P_{\mathrm{rat}}$ and $\mathrm{d}c_2/\mathrm{d}P_{\mathrm{rat}}$ in Eq. (A5) are determined as implicit functions of $\mathrm{d}a_p/\mathrm{d}P_{\mathrm{rat}}$ from Eqs. (A1) and (A2), respectively, and $\mathrm{d}P_{\mathrm{rat}}/\mathrm{d}c_2$ and $\mathrm{d}Q/\mathrm{d}c_2$ in Eq. (A6) are also determined in a similar manner as functions of $\mathrm{d}a_p/\mathrm{d}c_2$ from Eqs. (A1) and (A2).

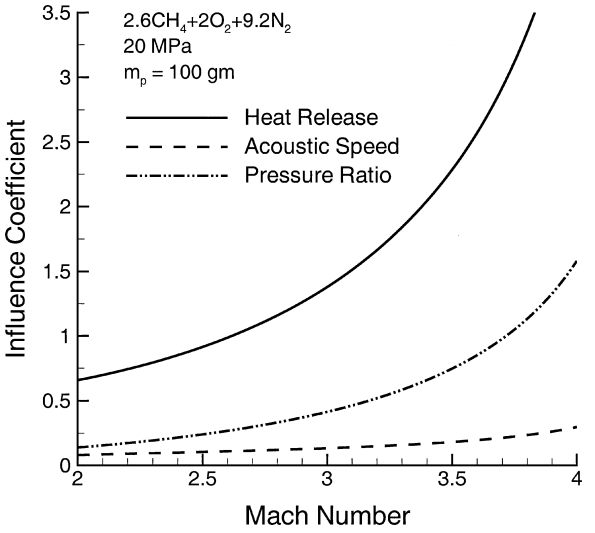

Fig. A1 Relative change in thrust coefficient as a result of real-gas effects on heat release, operating pressure ratio, and thermal choking acoustic speed.

The real-gas augmentation of the thrust coefficient is measured here by influence coefficients,[35] which indicate the relative change in thrust coefficient $\mathrm{d}I/I$ resulting from the relative changes in the heat release $\mathrm{d}Q/Q$, control volume pressure ratio $\mathrm{d}P_{\mathrm{rat}}/P_{\mathrm{rat}}$, or thermal choking point acoustic speed $\mathrm{d}c_2/c_2$, when using the Boltzmann equation of state rather than the ideal gas equation of state. From the definition of the thrust coefficient,

$$\mathrm{d}I = (m_p/P_1 A)\,\mathrm{d}a_p$$

Therefore, the relative change in the thrust coefficient as a result of heat release, pressure ratio, and acoustic speed are, respectively,

$$\left.\frac{\mathrm{d}I}{I}\right|_Q = \frac{m_p}{P_1 A}\left(\frac{Q}{I}\right)\left(\frac{\mathrm{d}a_p}{\mathrm{d}Q}\right)\left(\frac{\mathrm{d}Q}{Q}\right) \tag{A7}$$

$$\left.\frac{\mathrm{d}I}{I}\right|_{P_{\mathrm{rat}}} = \frac{m_p}{P_1 A}\left(\frac{P_{\mathrm{rat}}}{I}\right)\left(\frac{\mathrm{d}a_p}{\mathrm{d}P_{\mathrm{rat}}}\right)\left(\frac{\mathrm{d}P_{\mathrm{rat}}}{P_{\mathrm{rat}}}\right) \tag{A8}$$

$$\left.\frac{\mathrm{d}I}{I}\right|_{c_2} = \frac{m_p}{P_1 A}\left(\frac{c_2}{I}\right)\left(\frac{\mathrm{d}a_p}{\mathrm{d}c_2}\right)\left(\frac{\mathrm{d}c_2}{c_2}\right) \tag{A9}$$

The influence coefficient of a given parameter x is therefore of the form:

$$\frac{m_p}{P_1 A}\left(\frac{x}{I}\right)\left(\frac{\mathrm{d}a_p}{\mathrm{d}x}\right)$$

Because the derivatives of the acceleration are total derivatives, the interdependency of each of the thrust-affecting parameters is accounted for in each of the influence coefficients.[35] The influence coefficients for heat release, pressure ratio, and thermal choking acoustic speed are shown as functions of Mach number in Fig. A1, using the experimental conditions for $2.6CH_4 + 2O_2 + 9.2N_2$ propellant at 20 MPa, a projectile mass of 100 g, and a 38-mm ram accelerator tube bore.

The relative change in thrust coefficient as a result of real-gas effects on each of the parameters increases with Mach number for each of the thrust-affecting parameters. The values of the influence coefficients approach infinity as the Mach number approaches that of the CJ detonation wave, at which point the thrust coefficient is zero. From Fig. A1, it is apparent that a change in heat release causes the greatest relative change in the thrust coefficient (e.g., at $M = 3$, a 10% increase in the heat-release parameter causes a 14% increase in the thrust coefficient, a 10% increase in the pressure ratio causes a 4% increase in the thrust coefficient, and a 10% increase in the

thermal choking acoustic speed causes a 1.4% increase in the thrust coefficient). The thrust coefficient is considerably more sensitive to changes in heat release than pressure ratio or acoustic speed at all values of the Mach number in the range shown. Therefore, real-gas effects can be adequately incorporated into the unsteady thrust model by using the dependence of the heat-release parameter Q on Mach number that results from applying the Boltzmann equation of state. The other two influencing parameters are ignored at this time; however, means to include their effects in the one-dimensional thrust model under unsteady conditions are currently being developed.

Acknowledgments

This work was performed under U.S. Army Research Office Grant Number DAAG55-97-1-0131. The assistance of Liu Sen with the experiments is greatly appreciated.

References

[1]Hertzberg, A., Bruckner, A. P., and Bogdanoff, D. W., "Ram Accelerator: A New Chemical Method for Accelerating Projectiles to Ultrahigh Velocities," *AIAA Journal*, Vol. 26, No. 2, 1988, pp. 195–203.

[2]Bruckner, A. P., Burnham, E. A., Knowlen, C., Hertzberg, A., and Bogdanoff, D.W., "Initiation of Combustion in the Thermally Choked Ram Accelerator," *Shock Waves*, edited by K. Takayama, Springer-Verlag, Berlin, 1992, pp. 623–630.

[3]Schultz, E., Knowlen, C., and Bruckner, A. P., "Starting Envelope of the Subdetonative Ram Accelerator," *Journal of Propulsion and Power*, Vol. 16, No. 6, 2000, pp. 1040–1053.

[4]Bogdanoff, D. W., "Ram Accelerator Direct Space Launch System: New Concepts," *AIAA Journal of Propulsion and Power*, Vol. 8, No. 2, 1992, pp. 481–490.

[5]Knowlen, C., and Bruckner, A. P., "Direct Space Launch Using Ram Accelerator Technology," *Space Technology and Applications International Forum 2001*, edited by M. S. El-Genk, Springer-Verlag, New York, 2001, pp. 583–588.

[6]Bruckner, A. P., Knowlen, C., Hertzberg, A., and Bogdanoff, D. W., "Operational Characteristics of the Thermally Choked Ram Accelerator," *Journal of Propulsion and Power*, Vol. 7, No. 5, 1991, pp. 828–836.

[7]Knowlen, C., and Sasoh, A., "Ram Accelerator Performance Modeling," *Ram Accelerators*, edited by K. Takayama and A. Sasoh, Springer-Verlag, Heidelberg, 1998, pp. 25–37.

[8]Knowlen, C., and Bruckner, A. P., "A Hugoniot Analysis of the Ram Accelerator," *Shock Waves*, edited by K. Takayama, Springer-Verlag, Berlin, 1992, pp. 617–622.

[9]Bauer, P., Legendre, J. F., Henner, M., and Giraud, M., "Real Gas Effects in Ram Accelerator Propellant Mixtures: Theoretical Concepts and Applied Thermochemical Codes," *Ram Accelerators*, edited by K. Takayama and A. Sasoh, Springer-Verlag, Heidelberg, 1998, pp. 39–52.

[10]Bauer, P., Knowlen, C., and Bruckner, A. P., "Real Gas Effects on the Prediction of Ram Accelerator Performance," *Shock Waves*, Vol. 8, No. 2, 1998, pp. 113–118.

[11]Buckwalter, D. L., Knowlen, C., and Bruckner, A. P., "Real Gas Effects on Ram Accelerator Analysis," AIAA Paper 97-2894, July 1997.

[12]Buckwalter, D. L., Knowlen, C., and Bruckner, A. P., "Real Gas Effects on Thermally Choked Ram Accelerator Performance," *Ram Accelerators*, edited by K. Takayama and A. Sasoh, Springer-Verlag, Heidelberg, 1998, pp. 125–134.

[13]Bundy, C., Knowlen, C., and Bruckner, A. P., "Ram Accelerator Operating Characteristics at Fill Pressures Greater Than 10 MPa," AIAA Paper 99-2261, June 1999.

[14]Brouillette, M., Frost, D. L., Zhang, F., Chue, R. S., Lee, J. H. S., Thibault, P., and Yee, C., "Limitations of the Ram Accelerator," *Shock Waves at Marseille Vol. 1: Hypersonics, Shock Tube and Shock Tunnel Flow*, edited by R. Brun and L. Z. Dumitrescu, Springer-Verlag, Berlin, 1995, pp. 171–176.

[15]Bundy, C., Knowlen, C., and Bruckner, A. P., "Ram Accelerator Operation at Fill Pressures up to 20 MPa," AIAA Paper 2000-3231, July 2000.

[16]Bundy, C., "Effects of Unsteady Flow and Real Gas Equations of State on High Pressure Ram Accelerator Operation," Ph.D. Dissertation, Dept. of Aeronautics and Astronautics, Univ. of Washington, Dec. 2001.

[17]Shaw, B. D., and Wilbur, P. J., "The Annular Flow Electrothermal Ramjet," NASA Report CR-174704, July 1984.

[18]Owczarek, J., *Fundamentals of Gas Dynamics*, International Textbook Co., Scranton, PA, 1964, pp. 84–89.

[19]Bundy, C., Knowlen, C., and Bruckner, A. P., "Ram Accelerator Operating Characteristics at Elevated Fill Pressures," *Journal de Physique IV*, Vol. 10, Nov. 2000, pp. Pr11-11–Pr11-21.

[20]Knowlen, C., Bundy, C., and Bruckner, A. P., "Ram Accelerator Experiments Leading to Operation at Fill Pressures up to 20 MPa," AIAA Paper 2002-1015, Jan. 2002.

[21]Stewart, J. F., Knowlen, C., and Bruckner, A. P., "Effects of Launch Tube Gases on Starting of the Ram Accelerator," AIAA Paper 97-3175, July 1997.

[22]Stewart, J. F., Bruckner, A. P., and Knowlen, C., "Effects of Launch Tube Shock Dynamics on Initiation of Ram Accelerator Operation," *Ram Accelerators*, edited by K. Takayama and A. Sasoh, Springer-Verlag, Heidelberg, 1998, pp. 181–189.

[23]Schultz, E., Knowlen, C., and Bruckner, A. P., "Overview of the Subdetonative Ram Accelerator Starting Process," *Ram Accelerators*, edited by K. Takayama and A. Sasoh, Springer-Verlag, Heidelberg, 1998, pp. 189–203.

[24]Sasoh, A., Hamate, Y., and Takayama, K., "Small Bore Ram Accelerator Operation," *Journal of Propulsion and Power*, Vol. 17, No. 3, 2001, pp. 622–628.

[25]Li, C., and Kailasanath, K., "Initiation Mechanism of Thermally Choked Combustion in Ram Accelerators," *Journal of Propulsion and Power*, Vol. 15, No. 1, 1999, pp. 151–153.

[26]Schultz, E., Knowlen, C., and Bruckner, A. P., "Obturator and Detonation Experiments in the Subdetonative Ram Accelerator," *Shock Waves*, Vol. 9, No. 3, 1999, pp. 181–191.

[27]Giraud, M., Legendre, J. F., and Henner, M., "RAMAC in Subdetonative Propulsion Mode: State of the ISL Studies," *Ram Accelerators*, edited by K. Takayama and A. Sasoh, Springer-Verlag, Heidelberg, 1998, pp. 65–78.

[28]Sasoh, A., Hamate, Y., and Takayama, K., "Significance of Unsteadiness in Operation of the Small Bore Ram Accelerator," AIAA Paper 98-3446, July 1998.

[29]Hamate, Y., Sasoh, A., and Takayama, K., "Ram Accelerator Operations at Acceleration Level up to 6×10^4 g," *Journal de Physique IV*, Vol. 10, Nov. 2001, pp. Pr11-3–Pr11-9.

[30]Burnham, E. A., Kull, A. E., Knowlen, C., Bruckner, A. P., and Hertzberg, A., "Operation of Ram Accelerator in Transdetonative Velocity Regime," AIAA Paper 90-1985, July 1990.

[31]Hertzberg, A., Bruckner, A. P., and Knowlen, C., "Experimental Investigation of Ram Accelerator Propulsion Modes," *Shock Waves*, Vol. 1, No. 1, 1991, pp. 17–25.

[32]Higgins, A. J., Knowlen, C., and Bruckner, A. P., "Ram Accelerator Operating Limits, Part 1: Identification of Limits," *Journal of Propulsion and Power*, Vol. 14, No. 6, 1998, pp. 951–958.

[33]Higgins, A. J., Knowlen, C., and Bruckner, A. P., "Ram Accelerator Operating Limits, Part 2: Nature of Observed Limits," *Journal of Propulsion and Power*, Vol. 14, No. 6, 1998, pp. 959–966.

[34]Legendre, J. F., and Giraud, M., "Enhanced RAMAC Performance in Subdetonative Propulsion Mode with Semi-Combustible Projectile," *Journal de Physique IV*, Vol. 10, Nov. 2000, pp. Pr11-23–Pr11-30.

[35]Zucrow, M. J., and Hoffman, J. D., *Gas Dynamics, Vol. 1*, Wiley, New York, 1976, pp. 160–242.